Int J Adv Manuf Technol (2014) 73:147–159
DOI 10.1007/s00170-014-5763-1

ORIGINAL ARTICLE

Study of a hollow laser beam for cladding

Shuang Liu · Fanrong Kong · Shihong Shi · Radovan Kovacevic

Received: 28 October 2013 / Accepted: 6 March 2014 / Published online: 11 April 2014

Abstract Laser cladding, as a promising manufacturing technology, has been widely used in industry for component recovery and surface modification. In this paper, a hollow laser beam was proposed to optimize the laser intensity distribution. A three-dimensional (3-D) finite element (FE) model was developed using ANSYS to investigate the thermal field in the clad deposited by a hollow laser beam. The thermal results, such as the temperature distribution and the cooling rate, were investigated. The effect of the hollow ratio between the inner and outer radius of the hollow beam on the molten pool shape was also studied. The temperature at the boundary of the molten pool was higher than at the center. A clad with a flat metallurgical bonding was formed. The microstructure in the clad was mainly consisted of fine dendrites except the large columnar structures along the bonding. The hardness distribution of the clad was associated with the grain size distribution and the dilution by the substrate. The molten pool was not able to be generated with a high hollow ratio, while overheated at the center with a low hollow ratio. Based on the comparison with the Gaussian laser beam, the hollow laser beam could effectively alleviate the overheating at the center of the clad.

Keywords Hollow laser beam · Thermal field · Finite element analysis · Laser cladding

S. Liu · R. Kovacevic (✉)
Center for Laser-Aided Manufacturing, Southern Methodist University, 3101 Dyer Street, Dallas, TX 75205, USA
e-mail: kovacevi@lyle.smu.edu

F. Kong
ESAB Welding and Cutting, 411 S Ebenezer Rd, Florence, SC 29501, USA

S. Shi
School of Mechanical and Electrical Engineering, Soochow University, Suzhou 215021, China

1 Introduction

Laser cladding, as an efficient method for surface quality enhancement, has many advantages over the conventional welding-based surface modification methods, such as its highly localized heat input, low distortion of the workpiece, controllable dilution level, and fine grain size [1]. The coaxial powder injection method has been demonstrated to have superior flexibility and the best quality over the other methods [2].

In a typical laser cladding process, a focused solid laser beam encircled by several individual powder streams is used, as shown in Fig. 1a, b. The energy intensity is characterized by the highest value at the center and falling to $1/e^2$ of its peak at the boundary, which may result in overheating at the center while insufficient melting at the edge along the scanning path [3]. It is well known that dilution, as an important quality aspect of the clad, should be at a certain minimum value to guarantee a good interfacial bonding. The alloying of the clad with the substrate material can reduce the specific properties of the clad material. It is desired that the melting depth in the substrate to be small and close to a constant value over the diameter of the beam. The heat input over the width of the track should be uniform or increased at the edges, since the cooling rate at the edges is higher than at the center.

Beam shaping as a way to optimize the laser intensity distribution has been done in many laser material processing fields. A doughnut-shaped laser was widely used in the laser shock peening process, where an ultra-high intensity was required [4]. The shape of laser for texturing was changed from a Sombrero, a V-type donut, to a W-type donut, in order to control the friction and stiction behavior of the magnetic disk drives [5]. A ring-type beam and a rectangular V-type beam were proposed by Wang and Yang [6] to create the uniform hardened layer. Demirci et al. [7] developed a micro hollow laser beam system and found that it was a more efficient method for micro-manufacturing. In order to control

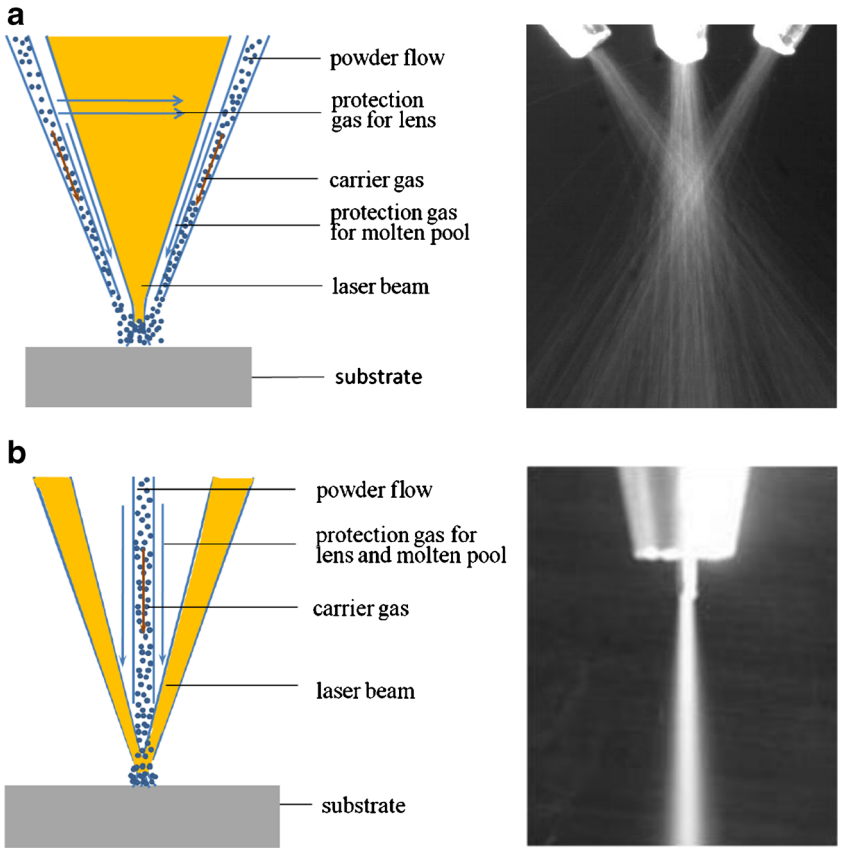

Fig. 1 **a** Solid laser beam cladding with its coaxial powder feeding nozzles, and **b** hollow laser beam cladding with its inner powder feeding nozzle

the dilution of the clad, Lange et al. [3] developed an optical system. Above the focal point, the energy intensity of the laser beam had a Gaussian distribution. Below the focal position, the energy intensity had a doughnut-shaped distribution. At the focal position, it had a top-hat distribution. They concluded that a uniform heat input over the track width could be achieved by a doughnut-shaped spot.

Shi and his co-workers [8] introduced a laser cladding technique by a hollow laser beam with an internal powder delivery system, as shown in Fig. 1b. This approach had a powder utilization above 60 % [9], which was more than twice of the coaxial powder feeding system. This feeding technique had several advantages with respect to the coaxial powder feeding system. First, a powder nozzle placed inside the laser beam formed a powder stream with a high concentration, resulting in the increase of the powder utilization. Second, the protection gas served multiple functions. Besides protecting the molten pool from oxidation, it also protected the lens from the contamination of plume and ricochet particles, and constricted the powder stream from divergence. Third, compared to the traditional solid Gaussian beam, the laser energy intensity with a hollow beam was effectively strengthened at the boundary of the laser spot and slightly weakened at its center.

Currently, most of the studies about the hollow laser beam are based on experimental results. Shi et al. studied [10] the influence of the laser defocused distance on the clad geometry, the hardness distribution and the microstructure characteristics. Li et al. [11] used the hollow laser beam to deposit a revolving body with variable diameters by controlling the laser power, the height increment, and the scanning speed. An internal wire feeding system has also been developed for component repair [12] and the generation of 3-D free-form structures [13]. Very few studies are available related to the in-process physical phenomena of the hollow beam cladding process. Due to the change of the laser beam shape, the temperature distribution of the molten pool is definitely changed. Consequently, the cooling rate, the microstructure, and the residual stress distributions are rearranged. However, because of the high energy intensity of the laser beam and the small size of the molten pool, it is extremely difficult to experimentally study the characteristics of the molten pool. Therefore, numerical simulation was used as a direct and effective way to study the thermal fields in the cladding process by a hollow laser beam. To date, only one paper had reported the results on the thermal field of the hollow laser beam cladding obtained by the finite element method. It assumed a uniform intensity distribution of the hollow beam and simplified the clad geometry to be brick-shaped [14].

Most of thermal analyses with finite element models were focused on the solid laser beam. The numerical models were developed from one-dimensional (1-D) [15], to two-

dimensional (2-D) [16], to three dimensional (3-D) [17]. The developed numerical models were verified experimentally, though some simplifications were made. All performed numerical and theoretical works largely help to understand the physical mechanisms involved in laser cladding.

In this study, in order to better understand the thermal behavior in the hollow laser beam cladding process, a 3-D thermo-mechanical finite element (FE) model was developed. The thermal results such as the temperature distribution and the cooling rate were investigated. The effect of the hollow ratio of the ring spot on the molten pool was also studied. The numerical work was verified by the experiments. The microstructure of the clad was investigated by an optical microscope (OM) and the hardness distribution across the clad was tested by a micro-hardness tester. The obtained results about the cladding by a hollow laser beam were compared with the results presented in the literature about cladding by a solid laser beam.

2 Experimental procedures

The Co-based alloy Stellite06 was deposited on a substrate of AISI304 by a hollow laser beam using a continuous wave CO_2 laser with a maximum power of 10 kW, as shown in Fig. 2. The composition and the physical properties of the clad material and the substrate were listed in Table 1. The processing parameters were a laser power of 4,000 W, a laser scanning speed of 3 mm/s, and a powder flow rate of 7.3 g/min. The clads were generated at the defocused distances where a ring laser spot was formed. For example, at the defocused distance of −4 mm, the outer diameter of the ring laser spot was 3.8 mm, and the inner diameter was 2.6 mm. The ratio between the inner and the outer diameter of the ring laser spot, called the hollow ratio, was 0.684. At the defocused distance of −7 mm, the outer diameter was 4.4 mm and the inner diameter was 3.2 mm. The hollow ratio was 0.727.

3 Numerical modeling

3.1 Thermal model

During laser cladding, the thermal equilibrium equation for a 3-D heat conduction of a moving heat source in a domain D, while considering that density ρ, thermal conductivity k, and specific heat c_p are temperature dependent, is given as [19]

$$\frac{\partial(\rho c_p T)}{\partial t} = \nabla.(k\nabla T) + \dot{Q} \quad (1)$$

where the physical properties of ρ, k, and c_p are given in Table 1, and $\dot{Q}$ is the heat generation rate. To obtain the solution from the thermal equilibrium equation, the boundary conditions and the initial conditions are needed.

The initial condition is

$$T(x,y,z,0) = T_0 \quad \text{for} \quad (x,y,z) \in D. \quad (2)$$

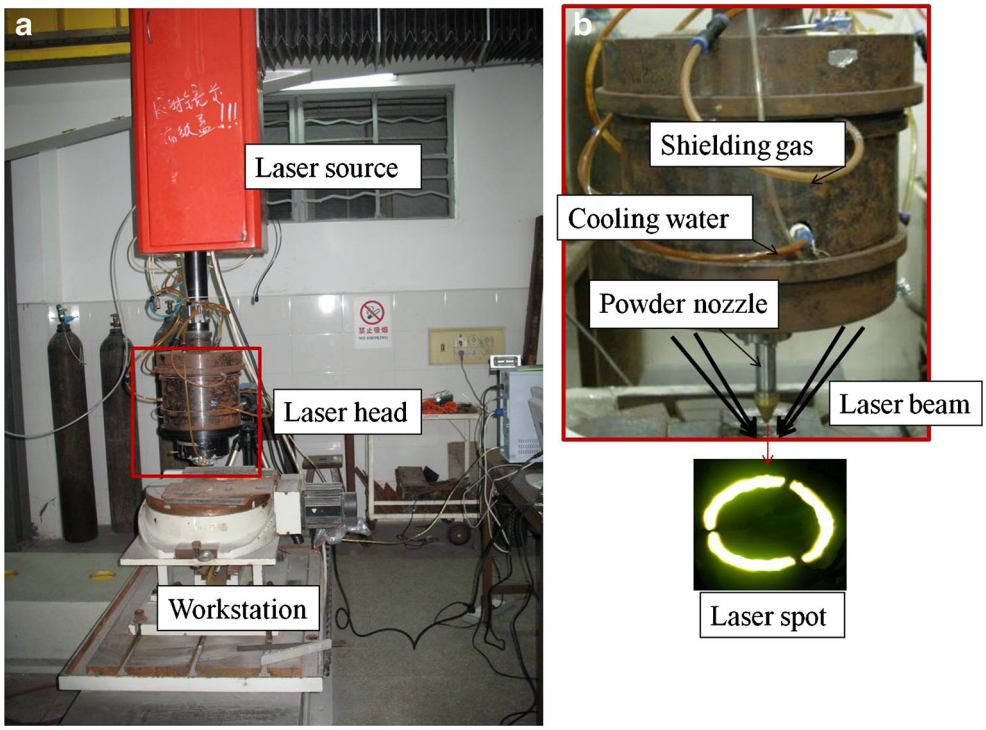

Fig. 2 **a** Experimental setup for laser cladding process and **b** internal powder injection system

Table 1 Composition and properties of AISI304 and Stellite06 [18]

Composition	C	Co	Cr	Fe	Mn	Mo	Ni	P		S		Si	
AISI 304	Max. 0.08	–	18~20	Bal.	Max. 2	–	8~10.5	Max. 0.045		Max. 0.03		Max. 1	
Stellite06	0.9~1.4	Bal.	28~32	Max. 3	Max. 2	Max. 1.5	Max. 3	–		–		Max. 2	
AISI 304													
T(K)	298	373	473	673	873	923	1,073	1,273	1,473	1,673	1,727	1,873	2,073
ρ(kg/m^3)	8,020		7,950	7,860	7,750		7,645	7,530	7,430	7,300	6,900	6,780	6,615
k(W/mk)	14.85		18.41	22.41	26.41		30.41	34.41	38.41	42.41		46.41	50.41
C_p(J/KgK)	500		535		616			696		776			856
α(μm/mk)		1.66E−05		1.79E−05		1.86E−05				2.08E−05			2.10E−05
L(J/g)	265.2												
E(Pa)	2.08E+11		1.95E+11	1.80E+11	1.50E+11		1.00E+11	1.00E+10	1.00E+10	1.00E+10	1000		1,000
λ	0.295		0.308	0.32	0.335		0.345	0.365	0.375	0.375	0.45		0.45
σ_y(Pa)	1.80E+08		1.30E+08	8.70E+07	6.40E+07		4.40E+07	1.70E+07	7.00E+06	7.00E+06			
σ_u(Pa)	5.86E+08		4.96E+08	4.39E+08	3.50E+08		2.00E+08	5.00E+07	5.00E+07	5.00E+07			
Stellite06													
T(K)	298	473	673	873	1073		1,473	1,628		1,901		2,073	
ρ(kg/m^3)	8,380												
k(W/mk)	14.85		22.41		30.41		38.41					50.41	
C_p(J/KgK)	456	482		573	629		741					909	
α(μm/mk)	1.39E−05		1.45E−05		1.58E−05			1.85E−05				1.85E−05	
L(J/g)	266												
E(Pa)	2.10E+11		1.65E+11		9.50E+10			2.73E+10		1,000		1,000	
λ	0.33		0.36		0.39			0.45		0.45		0.45	
σ_y(Pa)	6.40E+08		4.95E+08		2.80E+08			8.34E+07					
σ_u(Pa)	1.06E+09		1.00+09		5.00E+08			6.06E+07					

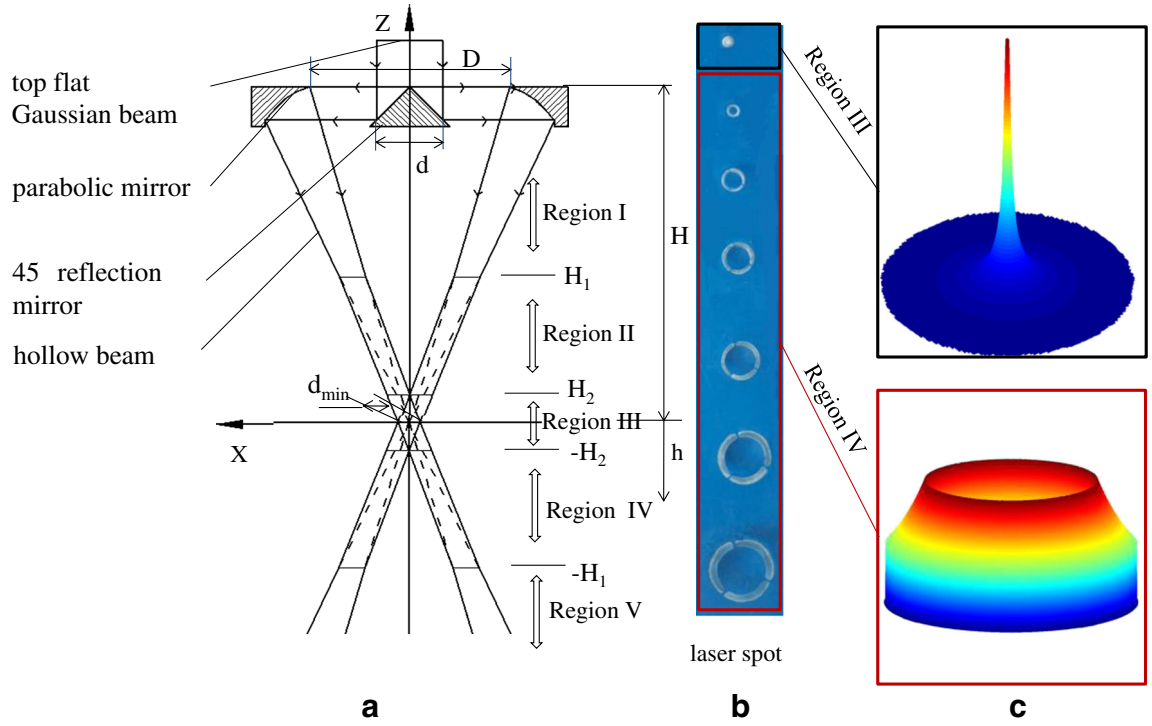

Fig. 3 **a** Schematic of hollow laser beam [20], **b** laser spot in region II and region III, and **c** energy density of the laser spot in region II and region III

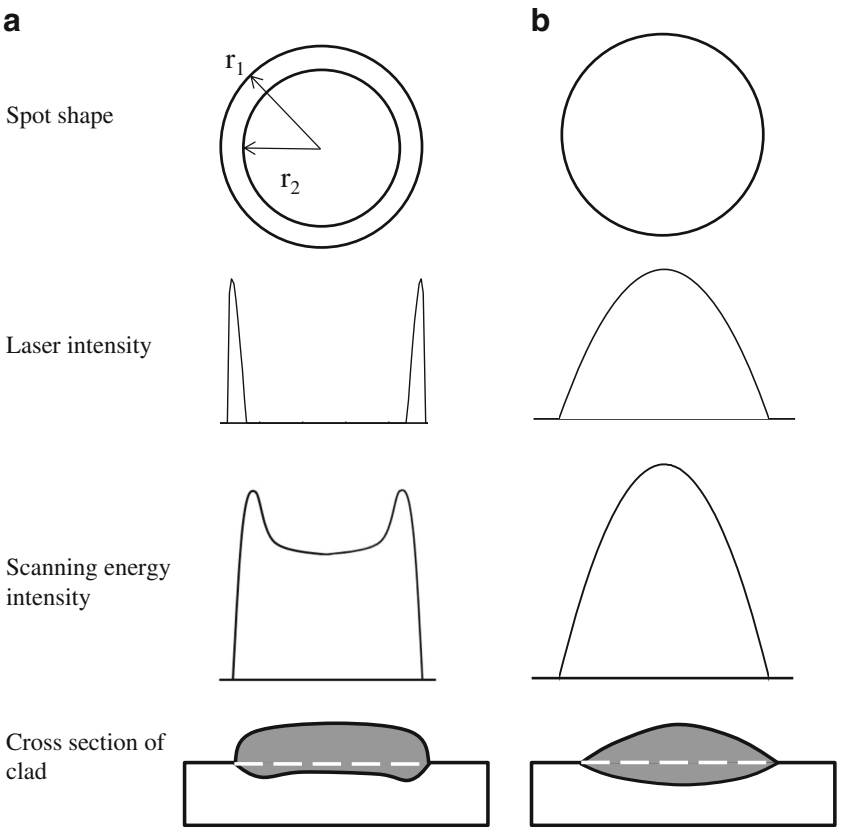

Fig. 4 Comparison between **a** a ring laser spot and **b** a solid laser spot

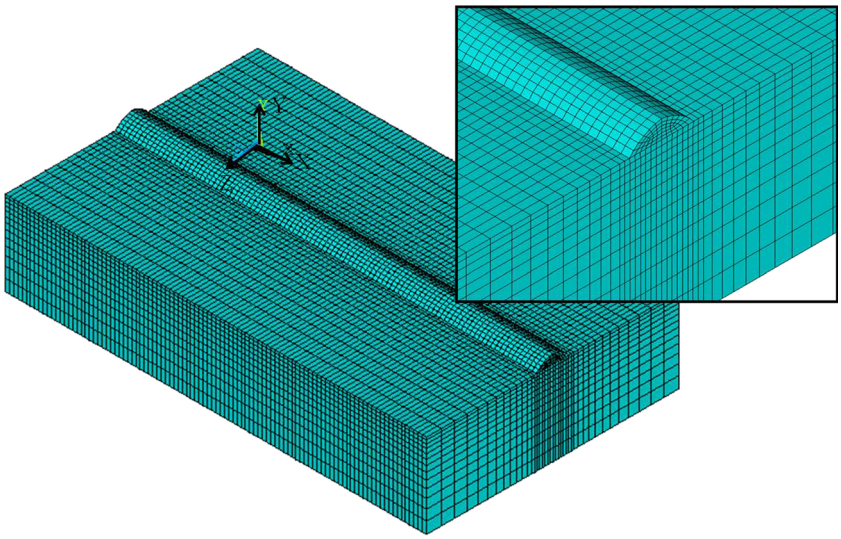

Fig. 5 FE mesh used in the simulation

The essential boundary condition is

$$T(x,0,z) = T_0 \tag{3}$$

on the boundary S_1 for $(x,z) \in S_1$ and $t>0$, where S_1 represents the bottom surface of the plate.

The natural boundary conditions can be defined by [17]

$$k_n \frac{\partial T}{\partial n} + h(T - T_0) + \sigma\varepsilon\left(T^4 - T_0^4\right) = 0 \tag{4}$$

on the boundary S_2 for $(x,y,z) \in S_2$ and $t>0$. S_2 represents those surfaces that are subjected to radiation, convection, and imposed heat fluxes.The effects of radiation and convection are combined into a "lumped" heat transfer coefficient. In the modeling, the heat transfer coefficient at the bottom of the surface was set at 120 W/(m^2•K) and at the sides at 40 W/(m^2•K) [17].

3.2 Heat source

Through a group of lenses, the cylindrical solid laser beam was transformed into a conical hollow laser beam. The schematic presentation of this beam is shown in Fig. 3a. It was assumed that the profile of the laser beam was symmetrical to the focal plane. The laser beam profile was divided into two parts: the straight propagation parts (region I and region V), and the Rayleigh range parts (region II, region III, and region IV). The laser spots in regions III and IV created on a plexiglass are shown in Fig. 3b. The energy intensity of the

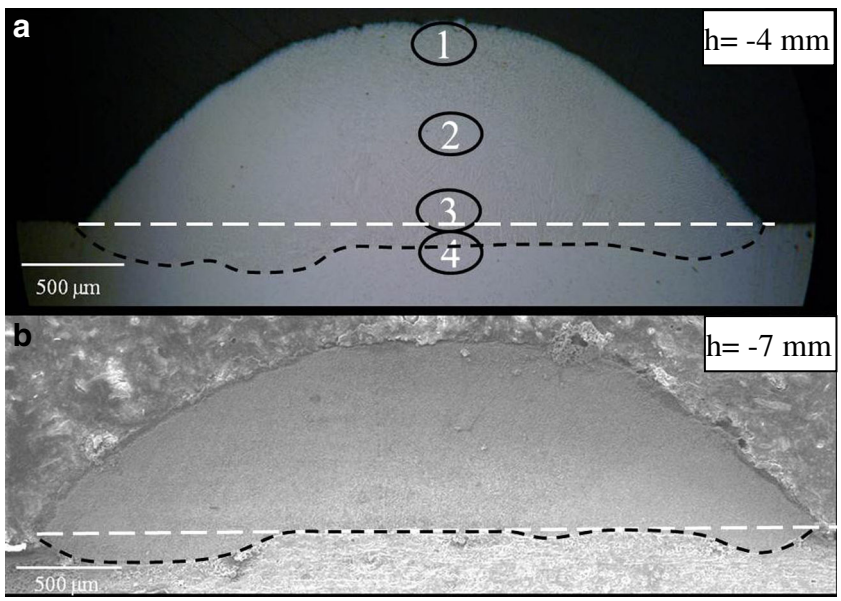

Fig. 6 The geometry of the clad generated at different defocused distances **a** h=−4 mm and **b** h=−7 mm

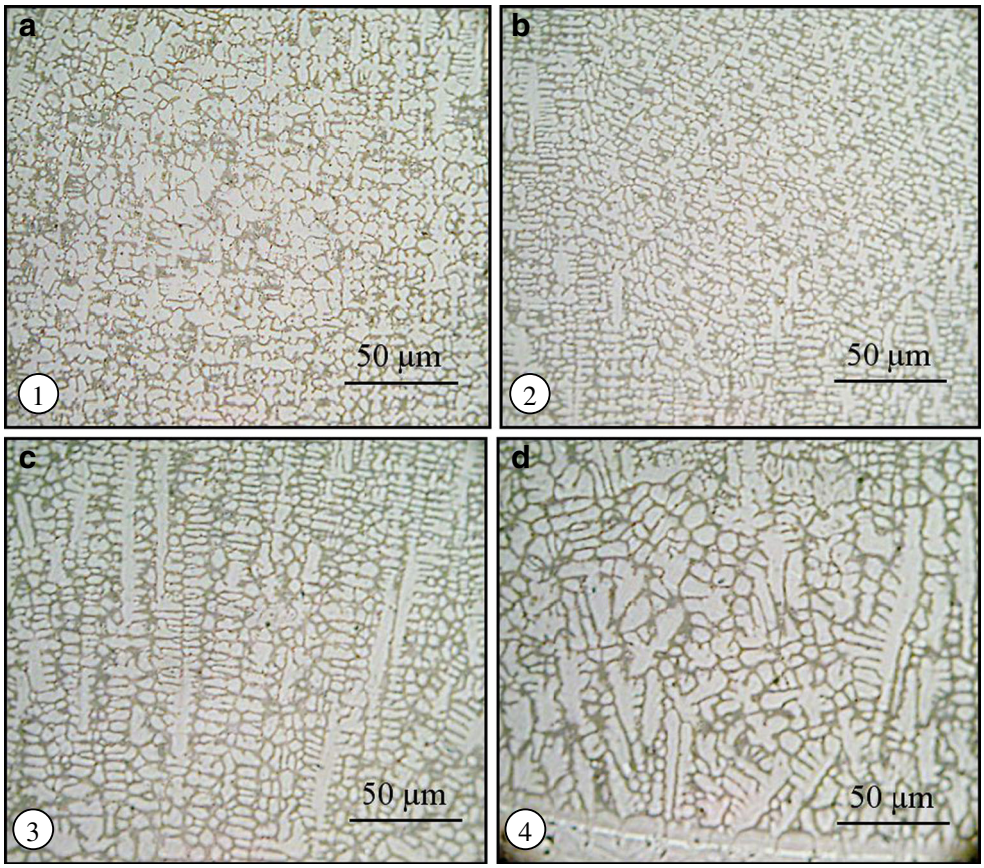

Fig. 7 Microstructure at **a** area 1, **b** area 2, **c** area 3, and **d** area 4

laser spot created in regions III and IV are plotted in Fig. 3c. Region II and region IV were primarily applied for cladding, because the energy densities in regions I and V were too weak while in region III was extremely high with a tiny laser spot.

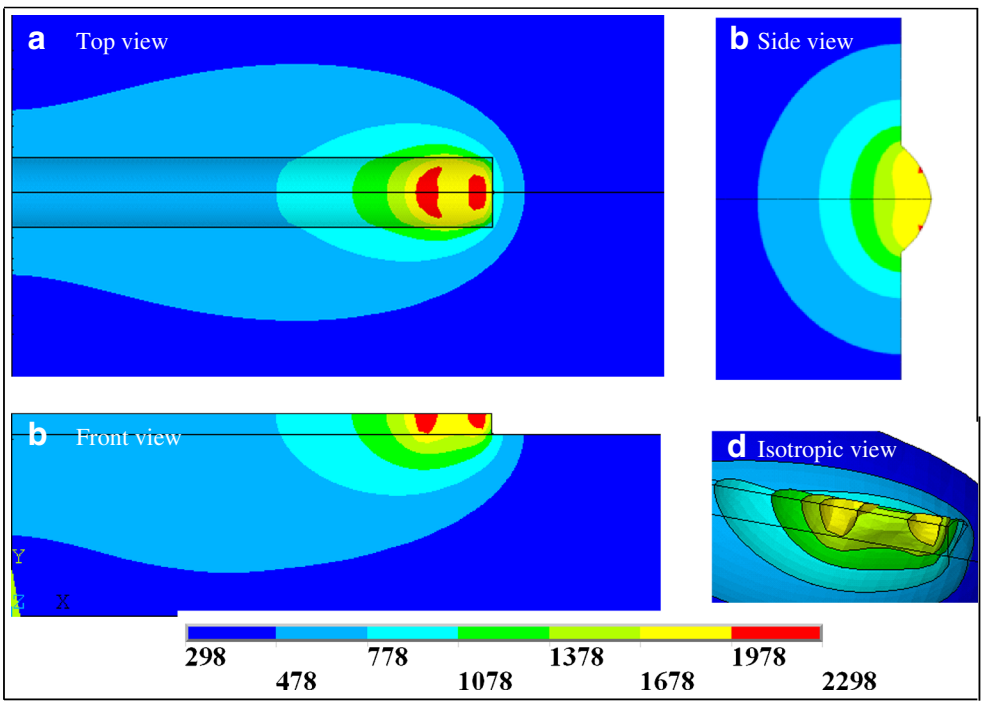

Fig. 8 Temperature contour images from **a** top view, **b** side view, **c** front view, and **d** isotropic view

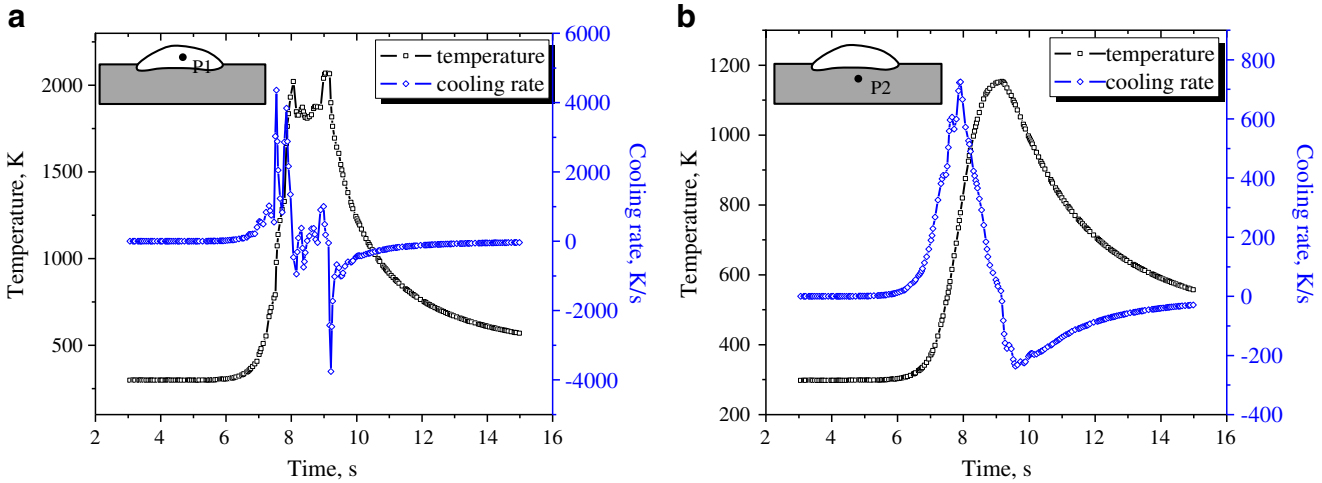

Fig. 9 Temperature histories and cooling rate evolutions: **a** at the center of the clad and **b** in the substrate out of the clad zone

The laser intensity distribution of the entire hollow laser beam was described in the "Appendix" section. Here, the only energy equation of region IV that was used for cladding is described by Eq. 5 [20]:

$$I = 2p\frac{\sqrt{2}H_1(a_1-H)a_1^2}{r|h|\left(a_1^2+2p^2\right)\left[\left(\sqrt{2}-1\right)|h|+H_1\right]}I_1 \tag{5}$$

where,

$$r\in\left(-\frac{d_{\min}}{2}+\frac{(H_1D+Hd_{\min})|h|}{2HH_1},\ \frac{d_{\min}}{2}+\frac{\left[H_1\left(p^2-\left(H-\frac{d}{2}\right)^2\right)-p\left(H-\frac{d}{2}\right)d_{\min}\right]|h|}{2p\left(H-\frac{d}{2}\right)H_1}\right),$$

$$a_1=\frac{p\left(b_1+\sqrt{b_1^2+H_1^2}\right)}{|H_1|},\ b_1=\frac{\sqrt{2}H_1r+\left(\frac{\sqrt{2}}{2}d_{\min}+\frac{D}{2H}H_1\right)(|h|-H_1)}{\left(\sqrt{2}-1\right)|h|+H_1},\ I_1 \text{ is the}$$

energy of the original solid laser beam, D is the diameter of the parabolic mirror, H is focal distance, $d_{\min}$ is the diameter of the focal spot, p is the characteristic parameter of the parabolic mirror, H_1 is half of the Rayleigh distance, H_2 is half of the intersection distance of the laser beam, h is the defocused distance, and r is the radius of the laser spot.

It must be noticed that the heat input at each point of the irradiated area could not be directly described by the laser intensity, but rather by the specific power per unit length along the cross direction (perpendicular to the scanning direction), which is also called the scanning energy intensity. That is to say, the scanning energy intensity could be obtained by the integration of the laser intensity along the scanning direction. For example, in the clad region IV, the laser spot was in a ring shape and the line intensity profile could be expressed as

$$E(x)=\begin{cases}2\int_{\sqrt{r_2^2-r^2}}^{\sqrt{r_1^2-r^2}}I(r)dr, & r_2\le r<r_1\\ 2\int_{0}^{\sqrt{r^2-r_2^2}}I(r)dr, & 0\le r<r_2\end{cases} \tag{6}$$

where r_1 and r_2 are the outer and inner radii of the ring spot, respectively.

In order to make a comparison between the hollow laser spot and the solid laser spot, the laser intensity, scanning energy intensity and the resulting cross-sections of the clads

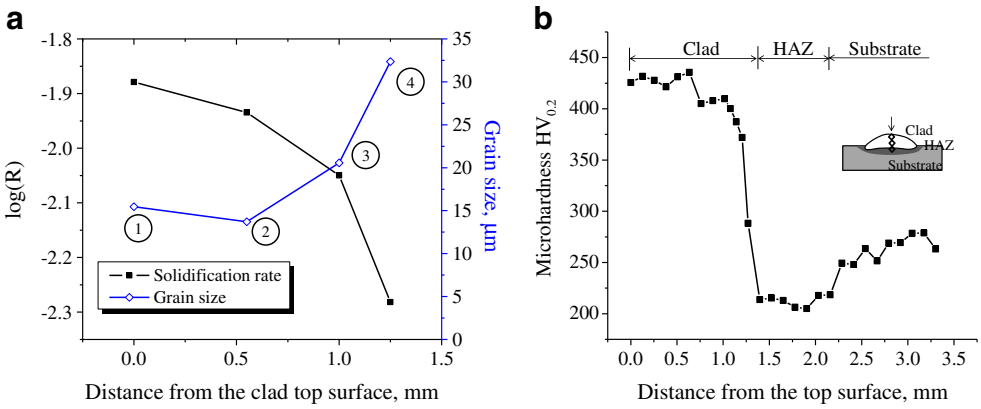

Fig. 10 **a** Grain size versus solidification rate and **b** the hardness distribution along the thickness of the clad

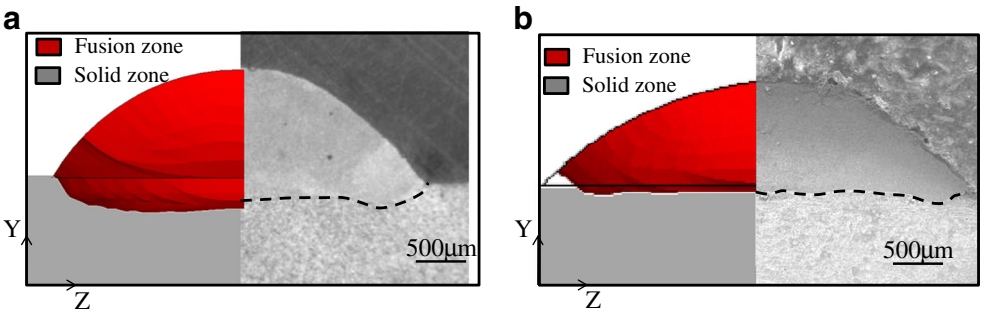

Fig. 11 The comparison of cross-sections of numerical simulation with the experimental results deposited at the defocused distance **a** H=−4 mm and **b** H=−7 mm

were plotted in Fig. 4a, b, respectively. The scanning energy intensity of the hollow laser beam was saddle-shaped, in which the energy at the center was attenuated while at the edge was enhanced. While, for the solid laser spot with a top-flat intensity distribution, the scanning energy intensity was higher at the center than at the boundary. For the hollow laser beam, the hollow ratio η was varied with the defocused distance and consequently affected the thermal field in the clad. Li [20] found that the hollow ratio η in the cladding region IV was in the range of 0.15~0.75.

3.3 Numerical implementation of thermal analysis

A nonlinear transient thermal model was developed using ANSYS. A nonuniform mesh was adapted to the zones of high thermal gradients, as shown in Fig. 5. The finest element size used in the clad zone was set at 0.2 mm, and a coarse mesh with element edge size up to 2 mm was used in the substrate far from the clad zone. Symmetry was considered at the middle plane along the direction of X. Hence, only half of the geometry was modeled. There were a total of 28,700 elements with 8-node brick SOLID70 in the thermal analysis [21]. The element "birth and death" option was used to simulate the additive nature of the process. In this method, the elements of the cladding layer were defined at the beginning of the process but "killed" by multiplying their stiffness (or conductivity, or other analogous quantity) by a severe reduction factor. According to the judgment of ANSYS parametric design language (APDL) at each time-step, the addition of the clad material was simulated by activating the elements of the cladding layer through removing the reduction factor [21].

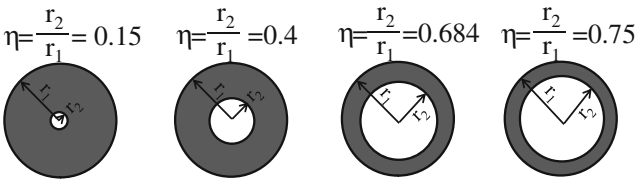

Fig. 12 Laser spot at different hollow ratios

4 Results and discussions

4.1 Typical microstructure of clad

Cross-sections of two clads created at the defocused distances of h=−4 mm and h=−7 mm are shown in Fig. 6a, b, respectively. The double-peaked melting interface could be clearly recognized. The microstructures of the clad at different positions as pointed out in Fig. 6a are shown in Fig. 7. The large columnar structures were predominated near the interface between the clad and the substrate. The regions at the center and near the top of the clad had a very fine dendrite structure. The characteristics of the microstructure in the clad were determined by the thermal gradient and the cooling rate in that area, which further affected the hardness distribution (see 4.2).

4.2 Thermal field

The thermal field of the clad deposited at h=−4 was predicted using the finite element method, as shown in Fig. 8. From top and front views, the highest temperatures were observed in the

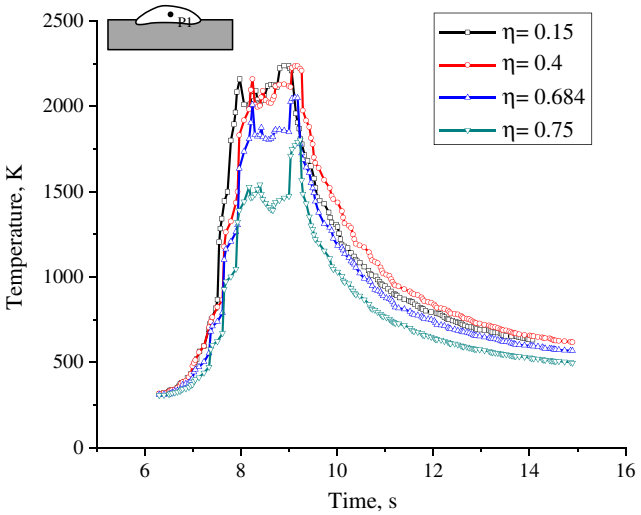

Fig. 13 Temperature history at the center of the clad with respect to different hollow ratios

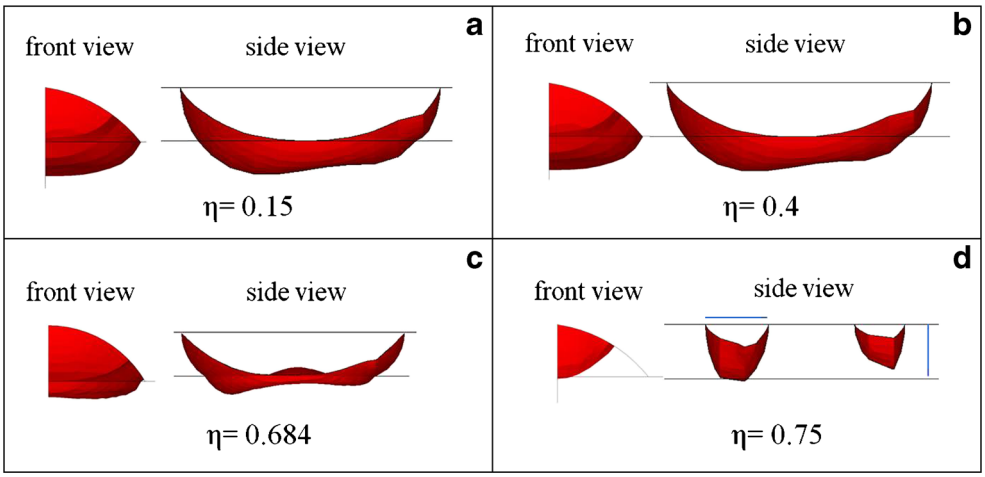

Fig. 14 Molten pool shapes at the hollow ratio: **a** η=0.15, **b** η=0.4, **c** η=0.684, and **d** η=0.75

front and the rear part of the molten pool. From the side view, it was found that the heat input near the edge of the track was enhanced by the hollow laser beam. The isotropic view shows that the molten pool was characterized with a "W" shape.

Two positions were selected to investigate the temperature history and the cooling rate: one at the center of the clad and the other at 2.5 mm below the former point in the substrate outside of the fusion zone. Figure 9a shows a two-peaked temperature profile at the center of the clad. The clad material was heated up by the front and the rear edges of the ring laser spot successively, whereas in the hollow part of the laser spot had a short cooling time. In the substrate out of the fusion zone, the heat transfer was mainly done by the thermal conduction from the clad. The evolutions of the temperature and the cooling rate are shown in Fig. 9b.

The grain morphology related to the solidification rate in the molten pool, is determined as [22]

$$R = \frac{\varepsilon}{G} \tag{7}$$

where ε is the cooling rate and G is the thermal gradient. Figure 10a shows that a higher solidification rate resulted in finer grains, and the grain size was distributed uniformly from the center to the boundary of the clad. It is known that the fine grain can improve the yield strength and the hardness of the material. The hardness was measured along the vertical line on the cross-section of the clad starting from the free surface to the substrate, as shown in Fig. 10b. The average hardness in the clad zone was about 420 $HV_{0.2}$. Due to the grain coarsening and the dilution with the substrate, the hardness in the clad close to the bonding was decreased to 290 $HV_{0.2}$. The heat affected zone (HAZ) in the substrate was softened to a hardness of 215 $HV_{0.2}$.

The thermal model was experimentally verified by comparing the isothermal image of the molten pool (at the left side) and the cross-section of the clad (at the right side) at the defocused distance H=−4 mm and H=−7 mm, as shown in Fig. 11a, b. The red zone at the left denotes the fusion zone, and the gray zone represents the nonmelted substrate. The isothermal boundary at the melting point of substrate AISI304 (1,678 K) was regarded as the molten pool edge. The dashed lines at the right side denote the bonding lines of the clad. It is evident that the simulation results had a good agreement with the experimental ones.

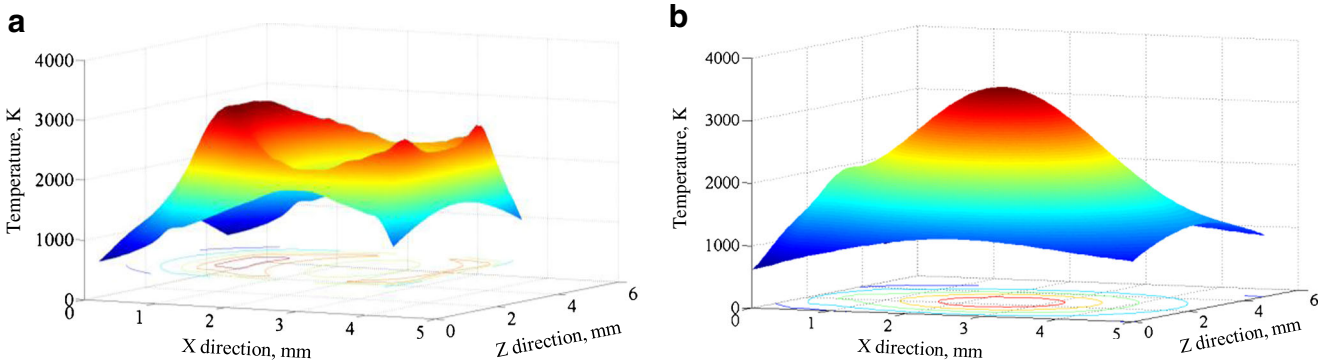

Fig. 15 Temperature distributions on the top surface of the molten pool created by **a** a hollow laser beam and **b** a solid laser beam

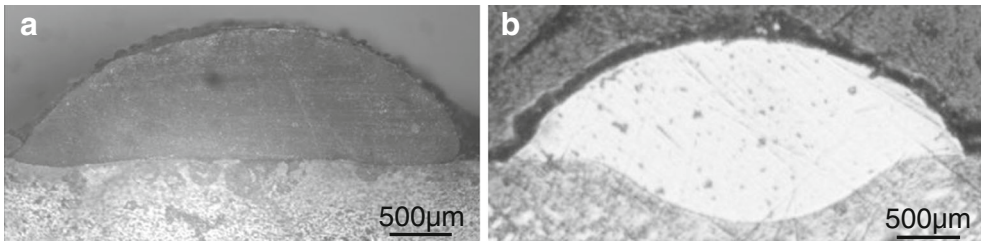

Fig. 16 Cross-sections of clad deposited by **a** a hollow laser beam and **b** a solid laser beam

4.3 Effect of the hollow ratio on the thermal field

In order to study the effect of hollow ratio of the ring laser spot on the thermal behavior, a case study was performed on the deposit of the single tracks with different hollow ratios. As mentioned before, the hollow ratios in the cladding region IV was in the range of 0.15~0.75. Hence, the hollow ratios of 0.15, 0.4, 0.684, and 0.75 were chosen, as shown in Fig. 12. The outer diameter of the laser spot was set at 3.8 mm, but its inner diameter was correspondingly changed from 0.57 to 2.85 mm. Figure 13 shows the variations of the temperature at the center of the clad with respect to time at different hollow ratios. The maximum temperature decreased with the increase in the hollow ratio. The larger the hollow ratio, the larger the difference of the temperature existed between at the center and at the boundary of the molten pool. When the hollow ratio was enlarged to 0.75, the energy concentrated only at the boundary of the ring laser spot and was not enough to melt the filler material. The front and side view of the molten pool at different hollow ratios are shown in Fig. 14. At hollow ratios of η=0.15 and 0.4, the melting depths were high, and the shape of the molten pool did not change too much. At η= 0.684, the molten pool became very flat and the dilution depth was low. At η=0.75, the molten pool of the clad was not formed. To sum up, a too small hollow ratio had minimal effects on the temperature uniformization of the molten pool, while a too large hollow ratio was not able to generate the molten pool. A hollow ratio close to 0.684 should be selected in the deposition. For deposition of the materials of Fe-based alloy and Ni-based alloy, the hollow ratio of 0.684 was used and good clads with flat bonding were also obtained.

4.4 Comparison of thermal fields between hollow and solid laser beam

In order to present the difference of the results generated by a hollow laser beam and a solid laser beam, a thermal model for a solid laser beam was developed and the corresponding experiment was also performed. The distributions of the surface temperature of the molten pool generated by the two laser sources are plotted in Fig. 15. The deposited clads are shown in Fig. 16. For the hollow laser beam cladding, the temperature along the boundary of the molten pool was higher than at the center. The dilution at the center of the clad was effectively alleviated and the metallurgical bonding near the boundary of the clad was improved accordingly. By contrast, for the solid laser beam the temperature at the center of the molten pool was highest, resulting in a deeper dilution at the center of the clad.

5 Conclusions

A hollow laser beam with an internal powder feeding technique was applied to surface cladding of Stellite 06 on the AISI304 substrate. The thermal field of the clad deposited by a hollow laser beam was numerically studied through a 3-D thermal FE analysis. The simulation model was verified by the experiment. The results achieved by the hollow laser beam were compared with the results obtained by the solid laser beam. Several conclusions could be drawn as follows:

1) A ring laser spot formed by a hollow laser beam was beneficial for enhancing the heat input at the boundaries of the molten pool. The hollow laser beam created a molten pool with a W-shaped interface with the substrate, characterized by a two-peaked temperature profile. Consequently, a clad that had a relatively flat interface with the substrate was obtained. In comparison, the molten pool obtained by a solid laser beam had a bowl-like shape with a deeper dilution at the center of the clad where the temperature was much higher than near the boundary.
2) The numerical model for the heat transfer in the clad obtained by the hollow laser beam was experimentally validated. The microstructure features and the hardness distribution of the clad were related to the thermal results of the model. The solidification rate decreased from the top surface of the clad to the metallurgical bonding with the substrate. As a result, large columnar crystals distributed along the interface and fine dendrite crystals located in the main clad area. The average hardness of the clad was 425 $HV_{0.2}$ and decreased to 290 $HV_{0.2}$ near the interface.
3) The hollow ratio was one of the critical factors used to determine the thermal field in hollow laser beam

cladding. A too small hollow ratio had minimal effects on the temperature uniformization of the molten pool, while a too large hollow ratio was not able to generate the molten pool. The hollow ratio near 0.684 was found to be the optimal one for achieving a clad with a flat metallurgical bonding.

Acknowledgments This work is sponsored by NSF Grant No. IIP-1034652 and by China's National Natural Science Grant No: 50975187 and 61078019. The first author would like to thank the laser manufacturing center in Soochow University for assistance in making the samples with a hollow laser.

Appendix

A cylindrical laser beam with the intensity I_0 irradiates a 45° mirror and is reflected onto a parabolic ring mirror, forming a hollow laser beam which is symmetrical to the focal plane, as shown in Fig. 3a. The laser beam profile is characterized by two parts: one is the straight propagation part of the laser (regions I and V) and the other is the Rayleigh range (regions II, III, and IV) when the laser beam is close to the focal point. In the Rayleigh range, the laser beam can be subdivided into two sections: one without intersections of the laser beam (regions II and IV) and one with intersections of laser beam (region III) [20].

In the straight propagation part (regions I and V), the distribution of the laser intensity I is written as [20]

$$I = 2p\frac{\sqrt{2}H_1(a_1-H)a_1^2}{r|h|\left(a_1^2+2p^2\right)}I_1 \tag{8}$$

where $r\in\left(\frac{p^2-\left(H-\frac{d}{2}\right)^2}{2p\left(H-\frac{d}{2}\right)|h|},\ \frac{D}{2H|h|}\right)$, $a_1=\frac{p\left(r+\sqrt{r^2+h^2}\right)}{|h|}$, p is the characteristic parameter of the parabolic mirror, h is the axis distance, H^1 is the Rayleigh length, and H^2 is the intersection length.

In the Rayleigh region without intersections of laser beam (regions II and IV), the distribution of laser intensity I yields as described in [20]

$$I = 2p\frac{\sqrt{2}H_1(a_1-H)a_1^2}{r|h|\left(a_1^2+2p^2\right)\left[\left(\sqrt{2}-1\right)|h|+H_1\right]}I_1 \tag{9}$$

where $r\in\left(-\frac{d_{\min}}{2}+\frac{(H_1D+Hd_{\min})|h|}{2HH_1},\ \frac{d_{\min}}{2}+\frac{\left[H_1\left(p^2-\left(H-\frac{d}{2}\right)^2\right)-p\left(H-\frac{d}{2}\right)d_{\min}\right]|h|}{2p\left(H-\frac{d}{2}\right)H_1}\right)$,
$a_1=\frac{p\left(b_1+\sqrt{b_1^2+H_1^2}\right)}{|H_1|}$, $b_1=\frac{\sqrt{2}H_1r+\left(\frac{\sqrt{2}}{2}d_{\min}+\frac{D}{2H}H_1\right)(|h|-H_1)}{\left(\sqrt{2}-1\right)|h|+H_1}$

In the Rayleigh region with intersections of laser beam (region III), the distribution of laser intensity I of the nonintersection part and intersection part are described as [20]

$$I = 2p\left(\frac{\sqrt{2}H_1(a_1-H)a_1^2}{r|h|\left(a_1^2+2p^2\right)\left[\left(\sqrt{2}-1\right)|h|+H_1\right]}+\frac{\sqrt{2}H_1(a_2-H)a_2^2}{r|h|\left(a_2^2+2p^2\right)\left[\left(\sqrt{2}-1\right)|h|+H_1\right]}\right)I_1 \tag{10}$$

where

$$r\in\left(0,\frac{d_{\min}}{2}-\frac{(H_1D+Hd_{\min})|h|}{2HH_1}\right),$$

$$a_1=\frac{p\left(b_1+\sqrt{b_1^2+H_1^2}\right)}{|H_1|},\quad b_1=\frac{\sqrt{2}H_1r+\left(\frac{\sqrt{2}}{2}d_{\min}+\frac{D}{2H}H_1\right)(|h|-H_1)}{\left(\sqrt{2}-1\right)|h|+H_1},$$

$$a_1=\frac{p\left(b_2+\sqrt{b_2^2+H_1^2}\right)}{|H_1|},\quad b_2=\frac{-\sqrt{2}H_1r+\left(\frac{\sqrt{2}}{2}d_{\min}+\frac{D}{2H}H_1\right)(|h|-H_1)}{\left(\sqrt{2}-1\right)|h|+H_1}$$

References

1. Toyserkani E, Corbin S, Khajepour A (2005) Laser cladding. CRC, Canada
2. Lowney M (2000) Nozzle particularly suited to direct metal deposition, United States, US Patent # 6,534,745
3. Lange D, Hofman J, Meijer J (2005) Influence of intensity distribution on the melt pool and clad shape for laser cladding. Proceedings of the Third International WLT-Conference on Lasers in Manufacturing, Munich
4. Fabbro R, Peyre P, Berthe L, Scherpereel X (1998) Physics and applications of laser-shock processing. J Las Appl 10(6): 265–280
5. Chilamakuri S, Bhushan B (1999) Contact analysis of laser textured disks in magnetic head-disk interface. Wear 230:11–23
6. Wang Y, Yang X, Liu Y (2006) Temperature field of laser scanning line facula. Chin J: Chin J Las 33(7):981–986

7. Demirci E, Nolke C, Kaierle S, Matteazzi P (2012) Development of a hollow laser beam for micromachining. Adv Opt Tech 1(5):365–370
8. Shi S and Fu G (2006) A laser cladding process with various laser spot sizes and its corresponding laser head configuration, China, CN Patent #200610024264.6
9. Shao Q (2008) Study on the technology of inside-laser coaxial powder feeding cladding and rapid prototyping process of laser. Ph.D. Thesis, Soochow University
10. Shi G, Shi S, Zhang J (2012) The influence of defocusing amount of hollow beam on the quality of single clad. Chin J : Appl Las 32(6): 505–509
11. Li H, Shi S, Fu G, Wang Y, Cai Q, Wang C, Sun H (2011) Control of process parameters of reducing solid of revolution with coaxial inside-beam powder feeding deposition. Chin J: Chin J Las 38(8): 3012–3024
12. Li C, Shi S, Liu S, Cai Q (2009) Roller repairing with intern coaxial wire feeding laser cladding. Chin J Hot Working Tech 38(18):3814–3819
13. Shi S, Fu G, Li L, Wang Y (2010) Realization and research of laser cladding with method of internal wire feeding through a hollow laser beam. Chin J: Chin J Las 1:266–270
14. Shi S, Wang C, Xu A, Sun H, Li H (2012) Temperature field numerical simulation of laser cladding based on internal powder feeding through a hollow laser beam. Chin J: Chin J Las 39(3):56–62
15. Chin R (1998) Thermomechanical modeling of residual stresses in layered manufacturing with metals. Ph.D.Thesis, Carnegie Mellon University
16. Deus A, Mazumder J (1996) Two-dimensional thermo-mechanical finite element model for laser manufacturing. International Congress on Applications of Lasers & Electro-Optics (Proc. ICALEO) 174–183
17. Labudovic M, Hu D, Kovacevic R (2003) A three dimensional model for direct laser metal powder deposition and rapid prototyping. J Mater Sci 38:35–49
18. Suarez A, Amado J, Tobar M, Yanez A, Fraga E, Peel M (2010) Study of residual stresses generated inside laser cladded plates using FEM and diffraction of synchrotron radiation. Surf Coat Tech 204: 1983–1988
19. Alimardani M (2009) Multi-physics analysis of laser solid freeform fabrication. Ph.D. Thesis, Univeristy of Waterloo
20. Li C (2010) Modeling for transmission and conversion of hollow circular laser and analysis on coupling between laser and materials in three-dimensional laser manufacturing. Ph.D. Thesis, Soochow University
21. Ansys 11.0, Structure and Thermal analysis
22. Dantzig J, Rappaz M (2009) Solidification methods microstructure and modeling, EPFL Press